RECOUPLING MULTI-TENSORIZED BOOST CONSISTENCY GRAPH LEARNING FOR INCOMPLETE MULTI-VIEW CLUSTERING

Anonymous authors
Paper under double-blind review

ABSTRACT

Incomplete multi-view clustering (IMVC) has grasped growing attention recently, which aims to address unsupervised clustering problems caused by missing views. While several method has been proposed, the current approaches still suffer from key shortcomings: Affinity graph learning methods based on Euclidean distances can be sensitive to feature magnitudes, leading to inadequately reflect informative relative response patterns. Moreover, existing methods recover missing view-specific information without considering cross-view diversity, resulting in suboptimal imputation. To overcome these challenges, we introduce a novel framework termed recoupling multi-tensorized boost consistency graph learning (RMTC-GL) for IMVC. Our approach first constructs correlation graphs using non-parametric Spearman correlation on complete samples, then recovers missing entries by preserving and leveraging all observed correlations via a masking strategy. To maintain view diversity, we incorporate a tensor-based diversity constraint that explicitly enforces heterogeneity among the recovered graphs across views. Additionally, we design a recomposed multi-tensor enhanced consensus learning module that jointly exploits cross-view complementarity for direct consensus graph recovery and captures high-order consistency between complete and incomplete correlation structures. Extensive experiments demonstrate that RMTC-GL achieves superior clustering accuracy compared to state-of-the-art methods.

1 INTRODUCTION

The proliferation of multi-view data in domains ranging from multimedia analysis to biomedical informatics has catalyzed the development of multi-view clustering techniques (Hu et al., 2025a;b), which aim to exploit the consensus and complementary information across different feature modalities to achieve superior clustering performance (Chen et al., 2025; Wang et al., 2025). However, a pervasive yet often overlooked obstacle is the prevalence of incomplete views, where certain samples are missing in one or more modalities. This incompleteness necessitates specialized IMVC approaches (Chen et al., 2026; Guo & Lu, 2024).

IMVC has emerged as an important problem, aiming to achieve reliable clustering by effectively handling missing views while preserving the complementary information across available views (Chen et al., 2022), which explicitly recovers missing views or missing representations before or during clustering and usually exploits cross-view correlations, subspace assumptions, or consensus constraints to infer the unavailable information (Ji et al., 2026a; Gu et al., 2026). For instance, BWIC-TIMC (Yao et al., 2025) jointly exploits between-view consistency and within-view correlations through tensor constraints for missing-view completion. ASCR (Xu et al., 2025) addresses IMVC by adaptively completing each view's missing anchor-sample similarities via a learned completion matrix. KOALA (Wu et al., 2025) handles uncoupled and incomplete data by learning cross-kernel alignment and applying low-rank tensor constraints to impute missing kernel elements.

Despite the progress in IMVC, several critical challenges remain. Conventional correlation graph construction may overlook nonlinear relationships among samples, resulting in an oversimplified characterization of complex data structures. Meanwhile, insufficient consideration of cross-view diversity during missing-information recovery may suppress view-specific patterns and compromise

Reviewers: please read the Reviewer Guidelines (iclr.cc/Conferences/2027/ReviewerGuidelines) and the AI Policy for Reviewers (iclr.cc/Conferences/2027/AIPolicyForReviewers). If you used AI to expand, edit, or polish your review, please provide the input text to the LLM. Better still, consider skipping the LLM and submitting your original text: we, and the authors, are much more interested in your unedited thoughts than in what an LLM has to say. AI-assisted or not, you are putting your name and reputation behind your review: LLM-generated falsehoods, hallucinations or misrepresentations are subject to disciplinary action, which may include desk-rejecting all papers you have authored.

recovery quality. Directly fusing incomplete graphs also fails to capture high-order interactions between view-specific graphs and the target consensus graph. Together, these issues hinder the learning of robust and structure-preserving representations from incomplete multi-view data. These challenges motivate a fundamental research question: *How can we reliably recover incomplete view-specific structures while preserving cross-view diversity and exploiting high-order consistency to learn a robust consensus graph?*

To address these limitations, we propose a novel framework termed recoupling multi-tensorized boost consistency graph learning for incomplete multi-view clustering. Specifically, we employ a non-parametric Spearman correlation to construct correlation graphs from complete samples, and when recovering missing graph entries, we fully leverage the intact information preserved in the original incomplete correlation graphs. Furthermore, we devise a tensor-based diversity constraint that explicitly enforces diversity among the recovered complete correlation graphs across views. Finally, we propose a recomposed multi-tensor enhanced consensus correlation learning framework, which not only exploits cross-view complementarity to directly recover a consensus correlation graph but also captures the high-order consistency between complete and incomplete correlation graphs. Collectively, these innovations enable more faithful, diverse, and structurally coherent graph recovery from incomplete multi-view data. The main contributions of this work are summarized as follows.

- We propose a novel IMVC method termed RMTC-GL, which integrates non-linear correlation graph construction, incomplete graph recovery, tensorial cross-view diversity embedding, and multi-tensor enhanced consensus graph learning into a unified framework.
- RMTC-GL builds view-specific graphs via Spearman correlation, recovers missing entries while preserving observed ones, and leverages tensor-based diversity and multi-tensor regularization to capture complementary information and high-order consistency.
- Extensive experiments on benchmark datasets demonstrate the effectiveness and robustness of RMTC-GL compared to various state-of-the-art methods.

2 Related Work

Existing IMVC methods can be discussed from three overlapping methodological perspectives: joint imputation and clustering, subspace representation learning, and graph learning (Zhang et al., 2023; Ji et al., 2026c). These perspectives emphasize different modeling mechanisms rather than mutually exclusive categories, since a framework may combine them (Gu et al., 2026).

Joint imputation methods couple missing-information recovery with the learning of clustering structures (Ji et al., 2026b). For example, IMSR (Liu et al., 2021) jointly optimize missing-data imputation and self-representation learning, allowing the learned coefficient matrix to guide data recovery. DIMIC (Li et al., 2022a) dynamically performs missing-view imputation and clustering by exploiting inter-view relationships. LaSA (Liu et al., 2024) primarily learns latent cluster-specific structures to guide missing-view recovery.

Subspace-based methods model relationships among samples through self-representation coefficients or learn compact latent representations from incomplete views (Li et al., 2022b; Tang et al., 2024). GUITAR (Zhong et al., 2026) integrates Gaussian regression, dual manifold regularization, and tensor rank minimization for robust IMVC. TLRADS (Cai et al., 2025) performs adaptive latent subspace representation learning and employs tensor subspace learning to capture high-order structural information across views. DATSL (Luo et al., 2026) performs discriminative subspace representation learning through non-convex low-rank regularization and category-aware distribution alignment, while GDATSL further preserves manifold structures via graph regularization.

Graph-based methods represent sample relationships through affinity graphs and address incomplete observations by recovering, refining, or fusing these structures (Liu et al., 2023; Cui et al., 2024; Li et al., 2025). RmoGL (Guo et al., 2025) decomposes self-representations into clean and noisy graphs and employs self-weighted fusion to learn a robust consensus graph. OGIMC (Zhou et al., 2024) completes missing graphs and fuses them into a consensus graph with adaptive view weights. CAL (Liu et al., 2025) applies structured sparse constraints to remove biased errors and leverages high-order tensor interactions under consensus guidance to learn a unified structural graph. SJSCG (Shu

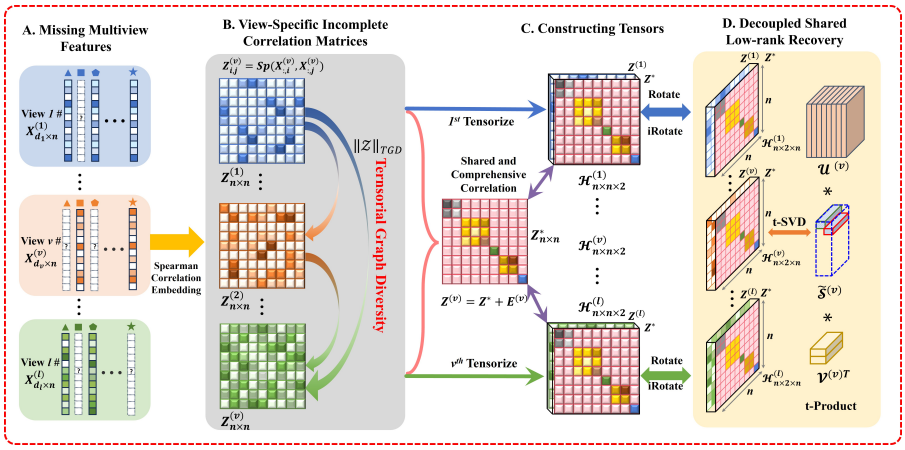

Figure 1: Overview of the proposed method.

et al., 2026) jointly learns a structure graph from incomplete data and a completion graph from recovered data, adaptively fuses them within each view, and aggregates view-specific fusion graphs into a consensus graph.

3 The Proposed Method

In this section, we will delve into the details of the proposed framework for IMVC problem. For clarity, the flowchart of the proposed approach is illustrated in Fig.1.

3.1 Partial Non-Linear Graph Construction

Euclidean distance measures pairwise proximity in the original feature space, but its reliance on absolute feature differences may limit its ability to characterize nonlinear dependencies and make it susceptible to feature redundancy and noise. We construct sample affinities by comparing the relative ordering of feature responses within each view, which captures nonlinear relationships without imposing assumptions on the underlying data distribution. For view v, let $\mathbf{X}_o^{(v)}{}_{(:,i)}$ denote the i-th observed sample, and let $\mathbf{r}_i^{(v)}$ denote its coordinate-wise rank vector, with average ranks assigned to ties. The Spearman correlation is defined as

$$\phi_{ij}^{(v)} = \frac{\left(\mathbf{r}_i^{(v)} - \bar{r}_i^{(v)}\mathbf{1}\right)^\top \left(\mathbf{r}_j^{(v)} - \bar{r}_j^{(v)}\mathbf{1}\right)}{\left\|\mathbf{r}_i^{(v)} - \bar{r}_i^{(v)}\mathbf{1}\right\|_2 \left\|\mathbf{r}_j^{(v)} - \bar{r}_j^{(v)}\mathbf{1}\right\|_2} \tag{1}$$

where $\bar{r}_i^{(v)}$ is the mean rank and $\phi_{ij}\left(\mathbf{X}_o^{(v)}\right) = Spearman\left(\mathbf{X}_o^{(v)}{}_{(:,i)}, \mathbf{X}_o^{(v)}{}_{(:,j)}\right)$. This correlation matrix serves as a similarity graph that robustly encodes the relational structure among samples. Then, we introduce the non-linear graph, which is defined as:

$$\mathbf{C}^{(v)} = \mathbf{G}^{(v)}\phi\left(\mathbf{X}_o^{(v)}\right)\mathbf{G}^{(v)T} \tag{2}$$

where $\mathbf{G}^{(v)}$ is a indicator matrix that maps the observed samples to their indices in the full dataset. $\mathbf{C}^{(v)}$ denotes the initial Spearman correlation graph computed from the observed data, providing an incomplete raw structure. Let $\mathbf{Q}_{ij}^{(v)} = 1$ when $i \neq j$ and both samples are observed in view v, and let $\mathbf{Q}_{ij}^{(v)} = 0$ otherwise. The mask distinguishes unavailable affinities from observed zero affinities. The recovered graph $\mathbf{Z}^{(v)}$ is learned through the masked residual $\mathbf{E}^{(v)} = (\mathbf{C}^{(v)} - \mathbf{Z}^{(v)}) \odot \mathbf{Q}^{(v)}$, which is then formulated accordingly:

$$\sum_{v=1}^{V} \left\|\mathbf{E}^{(v)}\right\|_1 = \sum_{v=1}^{V} \left\|\left(\mathbf{C}^{(v)} - \mathbf{Z}^{(v)}\right) \odot \mathbf{Q}^{(v)}\right\|_1 \tag{3}$$

3.2 TENSORIAL CROSS-VIEW GRAPH DIVERSITY EMBEDDING

During missing-information recovery, preserving cross-view diversity is essential because different views characterize the data from distinct perspectives and contain complementary, view-specific patterns. Excessive similarity among recovered graphs may suppress such discriminative information and introduce cross-view redundancy.

To balance information recovery and diversity preservation, we introduce a tensorial diversity constraint that encourages the recovered correlation graphs $\mathbf{Z}^{(v)}$ to retain view-specific structures while reducing redundant information across views.

Definition 1. *Let $\mathcal{Z} \in \mathbb{R}^{n_1 \times n_2 \times n_3}$ be a third-order tensor, then the Tensorial Graph Diversity (TGD) constraint can be defined as follows:*

$$\|\mathcal{Z}\|_{TGD} = \sum_{v=1}^{V} \sum_{w>v}^{V} \left\| \mathbf{Z}^{(v)} \odot \mathbf{Z}^{(w)} \right\|_1 = \sum_{v=1}^{V} \sum_{w>v}^{V} \mathrm{Tr}\left(\mathbf{Z}^{(v)} {\mathbf{Z}^{(w)}}^T \right) \tag{4}$$

where $\mathcal{Z} = \Psi\big([\mathbf{Z}^{(1)}, \mathbf{Z}^{(2)}, \cdots, \mathbf{Z}^{(V)}]\big)$ stacks the view-specific graphs into a third-order tensor. Minimizing this term penalizes high similarity between different views, effectively encouraging each view to retain its unique structural characteristics. This mechanism strikes a balance: the recovered graphs are neither forced to be identical nor allowed to diverge arbitrarily, leading to a set of view-specific graphs that are both complementary and diversity-preserving.

3.3 MULTI-TENSOR ENHANCED CONSENSUS GRAPH LEARNING

Existing approaches insufficiently model the high-order relationships between view-specific structures and the target consensus graph. Conventional full-graph tensor formulations stack the view-specific graphs into an $n \times n \times V$ tensor and apply t-SVD along the view dimension, requiring SVDs of $n \times n$ matrices in the Fourier domain.

To overcome these challenges, we propose a recouping multi-tensor enhanced consensus correlation graph learning strategy, which exploits cross-view complementarity to directly recover a consensus correlation graph $\mathbf{S}$ by minimizing: $\sum_{v=1}^{V} \left\| \mathbf{Z}^{(v)} - \mathbf{S} \right\|_F^2$, which aligns each view-specific recovered graph $\mathbf{Z}^{(v)}$ with a shared consensus graph $\mathbf{S}$, thereby fusing complementary information from all views. In addition, the method enforces high-order consistency between the complete and incomplete correlation graphs. For each view v, we stack the recovered graph $\mathbf{Z}^{(v)}$ and the shared consensus graph $\mathbf{S}$ into a two-slice tensor: $\mathcal{H}^{(v)} = \Psi\big([\mathbf{Z}^{(v)}, \mathbf{S}]\big)$, We then apply a tensor nuclear norm penalty to $\left\| \mathcal{H}^{(v)} \right\|_{\circledast}$. The high-order consistency is then enforced by imposing a low-rank tensor nuclear norm constraint on $\mathcal{H}^{(v)}$: $\sum_{v=1}^{V} \left\| \mathcal{H}^{(v)} \right\|_{\circledast}$.

Overall, the final objective is formulated as:

$$\begin{aligned}
&\min_{\mathbf{Z}^{(v)}, \mathbf{S}, \mathcal{H}^{(v)}} \sum_{v=1}^{V} \left\| \mathcal{H}^{(v)} \right\|_{\circledast} + \alpha \left\| \Big(\mathcal{C} - \mathcal{Z} \Big) \odot \mathcal{Q} \right\|_1 + \beta \sum_{v=1}^{V} \left\| \mathbf{Z}^{(v)} - \mathbf{S} \right\|_F^2 + \gamma \left\| \mathcal{Z} \right\|_{TGD} \\
&\text{s.t. } \phi_{i,j}\Big(\mathbf{X}_o^{(v)} \Big) = Spearman\Big({\mathbf{X}_o^{(v)}}_{(:,i)}, {\mathbf{X}_o^{(v)}}_{(:,j)} \Big), \quad \mathbf{C}^{(v)} = \mathbf{G}^{(v)} \phi\Big(\mathbf{X}_o^{(v)} \Big) {\mathbf{G}^{(v)}}^T, \\
&\quad \mathcal{C} = \Psi\big([\mathbf{C}^{(1)}, \cdots, \mathbf{C}^{(V)}]\big), \quad \mathcal{Z} = \Psi\big([\mathbf{Z}^{(1)}, \cdots, \mathbf{Z}^{(V)}]\big), \quad \mathcal{Q} = \Psi\big([\mathbf{Q}^{(1)}, \cdots, \mathbf{Q}^{(V)}]\big), \\
&\quad \mathcal{H}^{(v)} = \Psi\big([\mathbf{Z}^{(v)}, \mathbf{S}]\big), \quad \mathbf{Z}^{(v)} \geq 0, \quad diag(\mathbf{Z}^{(v)}) = 0, \quad \mathbf{Z}^{(v)} \mathbf{1} = \mathbf{1},
\end{aligned} \tag{5}$$

4 OPTIMIZATION

In this section, we solve Eq. (5) using an alternating optimization scheme based on the inexact augmented Lagrangian method (ALM). By introducing auxiliary constraints $\mathcal{J}^{(v)} = \mathcal{H}^{(v)}$, the aug-

mented Lagrangian is formulated as follows:

$$\begin{aligned}\mathcal{L}\Big(\Big\{\mathbf{Z}^{(v)}\Big\}_{v=1}^{V},\Big\{\mathcal{J}^{(v)}\Big\}_{v=1}^{V},\mathbf{S},\mathcal{E},\Big)&=\sum_{v=1}^{V}\Big\{\Big\langle\mathcal{T}^{(v)},\mathcal{H}^{(v)}-\mathcal{J}^{(v)}\Big\rangle+\frac{\rho}{2}\Big\|\mathcal{H}^{(v)}-\mathcal{J}^{(v)}\Big\|_F^2\\&+\Big\|\mathcal{J}^{(v)}\Big\|_{\circledast}\Big\}+\Big\langle\mathcal{K},\Big(\mathcal{C}-\mathcal{Z}\Big)\odot\mathcal{Q}-\mathcal{E}\Big\rangle+\frac{\lambda}{2}\Big\|\Big(\mathcal{C}-\mathcal{Z}\Big)\odot\mathcal{Q}-\mathcal{E}\Big\|_F^2+\alpha\left\|\mathcal{E}\right\|_1\\&+\sum_{v=1}^{V}\Big\{\beta\Big\|\mathbf{Z}^{(v)}-\mathbf{S}\Big\|_F^2+\gamma\sum_{w>v}^{V}\mathrm{Tr}\left(\mathbf{Z}^{(v)}{\mathbf{Z}^{(w)}}^{T}\right)\Big\},\end{aligned}\tag{6}$$

where $\rho>0$, $\lambda>0$ are the penalty factors, and $\mathcal{T}^{(v)}$, $\mathcal{K}$ denote Lagrange multipliers. All variables can be alternately updated as:

Updating S: Fixing the other variables and setting the derivative with respect to $\mathbf{S}$ to zero yields

$$\mathbf{S}_{t+1}=\frac{\sum_{v=1}^{V}\left[2\beta\mathbf{Z}_t^{(v)}+\rho_t\mathcal{J}_{(:,:,2),t}^{(v)}-\mathcal{T}_{(:,:,2),t}^{(v)}\right]}{V(2\beta+\rho_t)}.\tag{7}$$

Updating $\mathbf{Z}^{(v)}$: Fixing all variables except $\mathbf{Z}^{(v)}$ and setting the partial derivative with respect to $\mathbf{Z}^{(v)}$ to zero, then introducing the view missing information to correlation items, we can update for $\mathbf{Z}^{(v)}$ using the following:

$$\widehat{\mathbf{Z}_{ij}^{(v)}}=\frac{\mathbf{A}_{ij}^{(v)}+\mathbf{B}_{ij}^{(v)}}{2\beta+\rho+\lambda_t\mathbf{Q}_{ij}^{(v)}}\tag{8}$$

where $\mathbf{A}_{ij}^{(v)}=\Big(\lambda_t\mathbf{C}_{ij}^{(v)}-\lambda_t\Big(\mathbf{E}_{ij}^{v}\Big)_t+\Big(\mathbf{K}_{ij}^{(v)}\Big)_t\Big)\mathbf{Q}_{ij}^{(v)}$ and $\mathbf{B}_{ij}^{(v)}=2\beta(\mathbf{S}_{ij})_{t+1}-\gamma\sum_{w>v}^{V}\Big(\mathbf{Z}_{ij}^{(w)}\Big)_t-\Big(\Big(\mathcal{T}_{(:,:,1)}^{(v)}\Big)_{ij}\Big)_t$. The division is performed element-wise. The constrained solution is obtained by projecting each row onto the probability simplex:

$$\Big(\mathbf{Z}_{i,:}^{(v)}\Big)_{t+1}=\Pi_{\Delta_i}\left(\widehat{\mathbf{Z}}_{i,:}^{(v)}\right),\Delta_i=\left\{\mathbf{z}\geq 0:z_i=0,\ \mathbf{z}^T\mathbf{1}=1\right\},\tag{9}$$

where $\Pi_{\Delta_i}(\cdot)$ denotes the simplex projection (Wen et al., 2021).

Updating $\mathcal{E}$: Transforming variables into their corresponding multi-view representations, (6) is equivalent to the following compact formulation:

$$\mathbf{E}_{t+1}^{(v)}=\underset{\mathbf{E}^{(v)}}{\arg\min}\left(\frac{\alpha}{\lambda_t}\Big\|\mathbf{E}^{(v)}\Big\|_1+\frac{1}{2}\Big\|\mathbf{E}^{(v)}-\mathbf{Y}^{(v)}\Big\|_F^2\right)\tag{10}$$

where $\mathbf{Y}^{(v)}=\Big(\mathbf{C}^{(v)}-\mathbf{Z}_{t+1}^{(v)}\Big)\odot\mathbf{Q}^{(v)}+\mathbf{K}_t^{(v)}/\lambda_t$ is defined for notational simplicity. Inspired by soft-thresholding operator (Gao et al., 2020), the solution to the problem (10) is given by

$$\mathbf{E}_{t+1}^{(v)}=\mathrm{soft}_{\alpha/\lambda_t}\left((\mathbf{C}^{(v)}-\mathbf{Z}_{t+1}^{(v)})\odot\mathbf{Q}^{(v)}+\frac{\mathbf{K}_t^{(v)}}{\lambda_t}\right),\tag{11}$$

where $\mathrm{soft}_\tau(x)=\mathrm{sgn}(x)\max(|x|-\tau,0)$.

Updating $\mathcal{J}^{(v)}$: By removing the terms irrelevant to $\mathcal{J}^{(v)}$, the subproblem for $\mathcal{J}^{(v)}$ can be transformed into the following formulation:

$$\min_{\mathcal{J}^{(v)}}\Big\|\mathcal{J}^{(v)}\Big\|_{\circledast}+\frac{\rho_t}{2}\left\|\mathcal{J}^{(v)}-\mathcal{H}_{t+1}^{(v)}-\frac{\mathcal{T}_t^{(v)}}{\rho_t}\right\|_F^2.\tag{12}$$

In order to solve the low-rank tensor norm minimization problem (12), we introduce the following Theorem 1.

Theorem 1. *Given a third-order tensor $\mathcal{W}^{(v)} \in \mathbb{R}^{n_1 \times n_2 \times n_3}$ with tensor Fourier domain t-SVD $\overline{\mathcal{W}}^{(v)} = \overline{\mathcal{U}}^{(v)} * \overline{\mathcal{S}}^{(v)} * \overline{\mathcal{V}}^{(v)^T}$, for*

$$\arg\min_{\mathcal{J}^{(v)}} \zeta \left\| \mathcal{J}^{(v)} \right\|_{\circledast} + \frac{1}{2} \left\| \mathcal{J}^{(v)} - \mathcal{W}^{(v)} \right\|_F^2 \tag{13}$$

where $\zeta = \frac{1}{\rho}$ and $\mathcal{W}^{(v)} = \mathcal{H}_{t+1}^{(v)} + \frac{\mathcal{T}_t^{(v)}}{\rho}$. According to tensor-singular value thresholding (t-SVT) operator the optimal solution of $\mathcal{J}^{(v)}$ is

$$\mathcal{J}_{t+1}^{(v)} = \Gamma_\tau(\mathcal{W}^{(v)}) = \mathcal{U}^{(v)} * ifft\big(P_\tau\big(\overline{\mathcal{S}}^{(v)}\big)\big) * \mathcal{V}^{(v)^T} \tag{14}$$

where $\mathcal{U}^{(v)} = ifft\left(\overline{\mathcal{U}}^{(v)}, [], 3\right)$, $\mathcal{V}^{(v)} = ifft\left(\overline{\mathcal{V}}^{(v)}, [], 3\right)$ and $P_\tau\big(\overline{\mathcal{S}}^{(v)}\big)$ is an f-diagonal tensor, whose each diagonal elements can be learned in the GST algorithm (Yun et al., 2023). Consequently, optimal singular value $P_\tau\big(\overline{\mathcal{S}}^{(v)}\big)$ is constructed by $\mathbf{diag}\left\{\max(\overline{\mathcal{S}}_{(j,j)}^{(i)} - \tau, 0)\right\}$ *and* $i = 1, 2, \cdots, N$.

Therefore, the optimal solution of (12) is given as

$$\mathcal{J}_{t+1}^{(v)} = \Gamma_{\frac{1}{\rho}}\left(\mathcal{H}_{t+1}^{(v)} + \frac{\mathcal{T}_t^{(v)}}{\rho_t}\right) \tag{15}$$

Updating multipliers and penalty factors: Finally, the multipliers $\mathcal{T}^{(v)}$, $\mathcal{K}$ and penalty parameters ρ, λ are updated to satisfy the following constraints:

$$\begin{cases} \mathcal{T}_{t+1}^{(v)} = \mathcal{T}_t^{(v)} + \rho_t\big(\mathcal{H}_{t+1}^{(v)} - \mathcal{J}_{t+1}^{(v)}\big), \quad \mathcal{K}_{t+1} = \mathcal{K}_t + \lambda_t\big[(\mathcal{C} - \mathcal{Z}_{t+1}) \odot \mathcal{Q} - \mathcal{E}_{t+1}\big], \\ \rho_{t+1} = \min(\theta\rho_t, \rho_{\max}), \quad \lambda_{t+1} = \min(\theta\lambda_t, \lambda_{\max}). \end{cases} \tag{16}$$

The iterative optimization procedure stops when the convergence condition is satisfied. The stopping criteria are described as follows:

$$\left\| \mathcal{H}^{(v)}{}_{t+1} - \mathcal{J}^{(v)}{}_{t+1} \right\|_\infty \leq \epsilon_1, \forall v, \quad \left\| \Big(\mathcal{C} - \mathcal{Z}_{t+1}\Big) \odot \mathcal{Q} - \mathcal{E}_{t+1} \right\|_\infty \leq \epsilon_2 \tag{17}$$

where ϵ_1 and ϵ_2 are convergence constants.

Computational Complexity. We analyze the computational complexity of RMTC-GL. The main cost arises from constructing the initial Spearman correlation matrices, updating $\mathbf{S}$, $\mathbf{Z}^{(v)}$, $\mathbf{E}^{(v)}$, and $\mathcal{J}^{(v)}$, and computing the consensus spectral embedding $\hat{\mathbf{F}}$. Constructing the correlation matrices requires $\mathcal{O}(Vn_v d_v \log d_v + Vn_v^2 d_v)$, where V, n_v, and d_v denote the numbers of views, observed instances, and feature dimensions, respectively. Updating $\mathbf{S}$ and $\mathbf{Z}^{(v)}$ involves only basic matrix operations, while updating $\mathbf{E}^{(v)}$ costs $\mathcal{O}(n^2)$ per iteration. For $\mathcal{J}^{(v)}$, solving an $n \times 2 \times n$ tensor requires FFT, inverse FFT, and Fourier-domain SVD operations, resulting in $\mathcal{O}(2n^2 \log n + 4n^2)$ per view. After optimization, an SVD of the consensus matrix $\mathbf{S}$ is used to obtain the clustering representation, which costs $\mathcal{O}(n^3)$. Therefore, the overall complexity is $\mathcal{O}\big(Vn_v^2 d_v + 2Vn^2 \log(n)T + 2n^3\big)$.

Table 1: Summary of six benchmark datasets.

Datasets	Samples	Views	Clusters	Dimensions
BBC4	685	4	5	4659/4633/4655/4684
ALOI	1079	4	10	64/64/77/13
COIL	1440	3	20	6750/1024/3304
Leaves	1600	3	100	64/64/64
Caltech101-20	2386	6	20	48/40/254/1984/512/928
CCV	6773	3	20	20/20/20

5 EXPERIMENTS

5.1 EXPERIMENTAL SETUPS

Incomplete multi-view datasets: In our experiments, six real-world multi-view datasets are used to validate our RMTC-GL, consisting of text dataset BBC4 (Greene & Cunningham, 2006), object

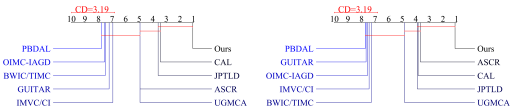

(a) ACC (b) NMI

Figure 2: Nemenyi tests across all datasets.

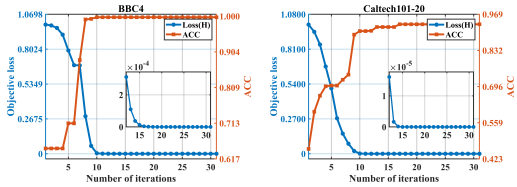

(a) BBC4 (b) Caltech101-20

Figure 3: Convergence on two datasets.

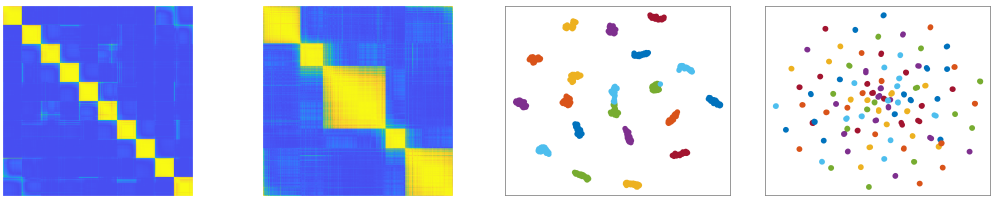

(a) ALOI (b) BBC4 (c) COIL (d) leaves

Figure 4: The t-SNE and heatmap visualization.

datasets ALOI (Geusebroek et al., 2005), COIL (Nene et al., 1996), image datasets Leaves (Beghin et al., 2010), Caltech101-20 [1], as well as video dataset CCV [2]. More details are shown in Table.1.

Compared methods: We compare RMTC-GL's clustering performance with nine SOTA methods: JPTLD (Lv et al., 2023), IMVC/CI (Tang et al., 2024), BWIC/TIMC (Yao et al., 2025), PBDAL (Li et al., 2025), CAL (Liu et al., 2025), ASCR (Xu et al., 2025), GUITAR (Zhong et al., 2026), UGMCA (Ma et al., 2026), OIMC-IAGD (Wu et al., 2026).

Evaluation metrics: Clustering performance is assessed using three standard metrics: ACC, NMI and Purity. Superior clustering performance is indicated by higher values of these evaluation metrics. The best results are highlighted in **bold**, and the second-best results are underlined.

Implementation: To construct incomplete multi-view data, a subset of $n \times mr$ entries is removed in the first view. For the second view, another missing entries are randomly removed, ensuring that no entries removed in the first view are removed again. For all remaining views, a similar random removal procedure entries is applied. To ensure a fair and reproducible comparison, we employ precisely grid search in ranges specified as optimal in the original paper for all methods.

5.2 Results Comparison and Analysis

Based on the comprehensive experimental results presented in Tables 2, the proposed method achieves the best or highly competitive performance across different datasets. Two key conclusions emerge: (1) Our method maintains near-perfect and stable performance as the missing rate rises to 50%, surpasses the second-best competitor in ACC by over 2% on ALOI, COIL, Leaves, and Caltech101-20. It also maintains ACC values above 99% on BBC4 and ALOI, confirming its ability to preserve reliable cluster assignments and structural consistency from incomplete data. (2) Our method performs effectively on both datasets with clear clustering structures and more complex heterogeneous datasets, while achieving substantial advantages on the more heterogeneous Caltech101-20 dataset, outperforming the second-best method by up to 18.92%, which demonstrates its strong adaptability to varying feature distributions.

We further conduct post-hoc Nemenyi tests based on the ACC and NMI rankings across the evaluated datasets. As shown in Figure. 2, RMTC-GL achieves the lowest average rank for both metrics. The results support the favorable average ranking of RMTC-GL, yet significant differences relative to comparisons are below the critical difference, CD $= 3.19$, at the 0.05 significance level.

[1] http://data.caltech.edu/records/mzrjq-6wc02

[2] http://www.ee.columbia.edu/ln/dvmm/CCV/

Table 2: Clustering results $[mean(std)]$ at different incomplete rates.

Dataset	Method/Rate	ACC			NMI			Purity		
		0.1	0.3	0.5	0.1	0.3	0.5	0.1	0.3	0.5
BBC4	JPTLD(TNNLS'23)	97.05(0.54)	96.83(0.60)	96.60(0.86)	94.36(0.32)	94.24(0.02)	94.21(0.42)	98.39(0.74)	98.25(0.99)	98.25(1.02)
	IMVC/CI(TNNLS'24)	86.16(0.65)	83.06(1.42)	79.47(1.88)	77.15(0.92)	72.88(1.38)	69.93(1.71)	91.97(1.23)	90.06(0.87)	88.18(1.56)
	BWIC/TIMC(TMM'25)	87.82(1.82)	83.65(2.05)	81.84(1.36)	70.59(1.13)	63.38(0.63)	60.05(1.71)	88.59(2.03)	87.78(0.93)	84.82(1.24)
	PBDAL(TMM'25)	65.16(0.65)	61.74(1.41)	45.19(1.80)	60.03(0.92)	53.44(1.28)	38.57(1.73)	76.46(1.64)	75.47(0.87)	56.07(2.56)
	CAL(IJCAI'25)	97.63(0.76)	96.21(1.19)	95.94(1.03)	94.32(1.57)	94.17(1.83)	91.83(2.06)	98.35(0.84)	97.88(1.28)	97.50(0.96)
	ASCR(AAAI'25)	98.94(0.41)	98.11(1.14)	97.78(1.93)	97.59(0.38)	96.41(0.69)	95.37(2.07)	99.42(1.64)	98.96(0.53)	98.69(0.77)
	GUITAR(NIPS'26)	79.82(1.53)	79.51(1.45)	73.00(1.04)	78.88(1.31)	75.65(1.22)	68.86(1.18)	88.74(1.43)	87.01(4.27)	83.61(1.99)
	UGMCA(TCE'26)	93.66(0.65)	92.53(1.42)	89.38(1.88)	88.73(0.92)	86.41(1.38)	82.82(1.71)	96.64(1.23)	95.91(0.87)	94.16(1.56)
	OIMC-IAGD(KBS'26)	74.51(5.95)	74.11(1.69)	72.53(2.02)	82.67(0.71)	82.46(2.78)	81.90(1.36)	75.89(4.93)	75.40(1.08)	73.96(2.18)
	Ours	**99.37(1.22)**	**98.41(0.35)**	**98.25(0.46)**	**99.42(0.41)**	**98.92(0.55)**	**98.07(1.46)**	**99.85(1.12)**	**99.72(0.68)**	**99.42(0.37)**
ALOI	JPTLD(TNNLS'23)	87.30(0.62)	84.29(0.91)	81.12(1.59)	87.89(0.58)	85.31(0.83)	83.16(1.27)	93.30(0.46)	91.53(0.71)	88.94(1.13)
	IMVC/CI(TNNLS'24)	68.55(0.49)	62.22(0.74)	60.38(1.16)	72.85(0.43)	68.23(0.68)	66.90(1.04)	82.86(0.37)	77.16(0.52)	76.13(0.86)
	BWIC/TIMC(TMM'25)	48.45(0.85)	46.31(1.06)	45.93(1.34)	59.29(0.72)	58.03(0.93)	56.84(1.21)	63.21(0.64)	61.16(0.81)	59.65(1.08)
	PBDAL(TMM'25)	47.35(0.41)	36.27(0.39)	31.72(0.14)	55.70(0.57)	47.52(0.75)	40.53(0.65)	55.11(1.10)	49.32(2.04)	44.81(0.11)
	CAL(IJCAI'25)	94.69(0.86)	94.35(2.03)	93.99(0.61)	94.68(0.20)	94.61(1.27)	94.45(1.73)	97.28(0.45)	97.12(0.70)	96.93(0.48)
	ASCR(AAAI'25)	74.03(3.08)	73.89(3.08)	70.79(1.56)	81.17(1.15)	80.83(1.91)	80.77(0.28)	78.83(3.12)	78.30(2.96)	74.44(0.76)
	GUITAR(NIPS'26)	67.02(2.11)	63.54(2.57)	59.30(1.82)	71.20(1.37)	68.30(2.41)	62.50(1.45)	74.45(3.72)	70.20(2.47)	69.50(4.24)
	UGMCA(TCE'26)	80.21(1.76)	80.94(0.95)	79.50(1.40)	91.57(1.51)	91.71(0.44)	90.97(1.18)	85.68(0.97)	85.43(1.49)	84.69(1.32)
	OIMC-IAGD(KBS'26)	71.95(2.69)	68.23(1.65)	64.27(1.17)	78.27(2.03)	76.33(0.72)	71.07(1.87)	86.47(1.44)	84.14(0.98)	79.09(0.52)
	Ours	**98.05(1.23**	**97.58(0.31)**	**95.26(1.38)**	**99.54(0.36)**	**98.91(0.31)**	**97.96(0.43)**	**99.81(1.11)**	**99.54(0.19)**	**99.07(0.58)**
COIL	JPTLD(TNNLS'23)	81.41(0.75)	80.25(0.83)	79.42(0.31)	89.06(0.23)	89.02(0.28)	88.51(0.18)	83.22(0.63)	82.00(0.90)	81.23(0.29)
	IMVC/CI(TNNLS'24)	80.34(0.62)	80.08(0.84)	79.12(0.31)	92.01(2.14)	91.66(0.61)	89.03(2.25)	83.51(0.68)	82.92(0.58)	82.49(2.02)
	BWIC/TIMC(TMM'25)	47.74(3.02)	34.60(1.09)	29.00(1.81)	73.41(1.33)	64.34(0.73)	59.72(0.82)	65.78(2.08)	58.02(1.37)	55.63(1.40)
	PBDAL(TMM'25)	28.49(0.41)	25.59(1.61)	25.25(0.96)	54.53(0.23)	43.27(0.43)	38.80(1.10)	43.44(0.72)	36.27(1.06)	32.93(1.51)
	CAL(IJCAI'25)	73.72(0.43)	72.30(0.70)	69.24(2.48)	85.76(0.29)	84.75(0.04)	83.53(1.04)	78.78(0.29)	77.19(0.38)	73.14(2.44)
	ASCR(AAAI'25)	71.20(1.51)	70.95(1.57)	70.94(0.98)	82.93(0.73)	82.69(0.74)	82.60(0.59)	75.90(0.95)	75.90(1.53)	75.45(1.07)
	GUITAR(NIPS'26)	74.11(1.69)	72.53(2.02)	74.51(5.95)	82.67(0.71)	81.90(1.36)	82.46(2.78)	75.40(1.08)	73.96(2.18)	75.89(4.93)
	UGMCA(TCE'26)	68.51(1.48)	63.96(0.87)	58.61(1.62)	84.97(0.92)	83.07(1.34)	79.98(0.76)	70.49(1.23)	64.33(0.95)	62.85(1.56)
	OIMC-IAGD(KBS'26)	66.77(3.39)	65.91(2.83)	64.58(1.48)	80.56(1.70)	79.12(0.89)	79.01(1.70)	72.20(3.77)	71.60(1.90)	71.49(1.99)
	Ours	**87.52(0.43)**	**86.51(0.59)**	**85.26(1.08)**	**96.51(0.19)**	**92.56(0.30)**	**89.56(0.37)**	**88.81(0.72)**	**86.72(0.86)**	**86.23(0.76)**
Leaves	JPTLD(TNNLS'23)	88.91(2.16)	85.85(1.20)	84.64(1.93)	96.39(0.57)	95.53(0.41)	95.01(0.64)	89.86(1.97)	87.79(1.53)	87.21(1.68)
	IMVC/CI(TNNLS'24)	75.17(1.12)	68.17(1.24)	61.95(0.76)	91.03(0.34)	87.76(0.39)	85.10(0.31)	83.15(1.19)	78.65(1.55)	74.83(0.98)
	BWIC/TIMC(TMM'25)	79.55(1.13)	74.30(0.96)	65.78(1.23)	92.50(0.26)	90.31(0.32)	86.50(0.43)	85.79(0.83)	83.03(1.40)	77.43(1.13)
	PBDAL(TMM'25)	86.74(0.89)	86.74(0.57)	84.16(1.02)	95.99(0.88)	95.80(0.30)	93.13(0.69)	89.46(0.43)	89.33(0.64)	86.69(1.47)
	CAL(IJCAI'25)	90.13(0.34)	89.16(0.96)	88.09(0.21)	96.69(1.07)	96.54(1.89)	96.31(0.69)	90.23(0.82)	89.70(1.27)	88.65(0.55)
	ASCR(AAAI'25)	81.22(1.72)	80.33(0.56)	80.17(0.52)	95.10(0.11)	93.90(0.66)	93.04(0.13)	84.25(0.45)	84.17(1.58)	83.72(0.38)
	GUITAR(NIPS'26)	74.29(0.72)	65.56(0.10)	65.26(1.15)	87.85(0.83)	81.05(0.22)	80.91(1.96)	77.19(1.36)	67.97(1.94)	68.14(0.16)
	UGMCA(TCE'26)	90.42(0.47)	88.66(0.66)	88.52(0.76)	96.76(0.24)	95.97(0.33)	96.01(0.29)	92.81(0.38)	91.81(0.52)	90.81(1.69)
	OIMC-IAGD(KBS'26)	70.17(1.93)	56.37(2.02)	41.48(1.26)	86.75(0.70)	76.66(0.71)	67.98(0.44)	73.31(1.67)	58.97(1.74)	44.25(0.85)
	Ours	**98.46(0.23)**	**97.28(0.29)**	**93.36(0.45)**	**99.53(0.05)**	**99.30(0.07)**	**97.97(0.14)**	**98.65(0.18)**	**97.76(0.22)**	**94.80(0.34)**
Caltech101-20	JPTLD(TNNLS'23)	56.54(1.85)	55.94(1.77)	53.17(3.52)	74.80(0.69)	73.90(1.00)	73.03(0.98)	64.13(1.64)	64.05(1.69)	61.81(2.97)
	IMVC/CI(TNNLS'24)	45.99(0.73)	45.56(0.68)	45.35(0.92)	59.89(0.53)	58.69(0.47)	56.53(0.86)	51.57(0.95)	51.42(1.03)	51.20(2.52)
	BWIC/TIMC(TMM'25)	68.08(3.35)	66.41(1.05)	65.63(0.83)	77.39(1.19)	72.21(1.12)	72.14(0.86)	69.18(1.31)	69.13(2.29)	68.50(4.21)
	PBDAL(TMM'25)	59.46(0.81)	57.73(1.03)	53.24(1.13)	72.19(0.35)	71.48(0.95)	68.97(0.74)	88.02(1.10)	86.75(0.68)	86.24(0.95)
	CAL(IJCAI'25)	71.78(1.54)	67.39(1.81)	67.03(1.93)	70.06(1.68)	66.13(1.97)	66.14(1.85)	74.26(1.04)	70.89(0.48)	69.91(0.72)
	ASCR(AAAI'25)	60.77(0.52)	55.87(0.48)	54.23(0.48)	77.85(0.16)	77.73(0.17)	75.62(0.17)	85.54(0.31)	85.39(0.35)	83.32(0.35)
	GUITAR(NIPS'26)	59.48(0.41)	57.13(0.02)	51.70(1.08)	71.25(1.52)	67.53(0.75)	60.64(0.91)	84.69(1.24)	81.67(0.18)	75.10(1.22)
	UGMCA(TCE'26)	63.86(0.65)	63.35(1.41)	57.32(1.89)	71.57(0.92)	70.48(1.28)	67.28(1.73)	68.52(1.34)	68.15(0.87)	62.41(1.56)
	OIMC-IAGD(KBS'26)	61.78(0.73)	61.03(1.16)	59.12(0.92)	63.09(0.22)	60.48(0.44)	57.92(0.33)	75.94(0.17)	76.18(0.38)	73.85(0.27)
	Ours	**88.70(1.85)**	**87.07(1.61)**	**79.37(1.15)**	**90.10(0.75)**	**88.21(1.02)**	**84.84(0.69)**	**91.74(1.31)**	**89.37(1.41)**	**88.84(1.51)**
CCV	JPTLD(TNNLS'23)	47.33(0.05)	45.61(0.39)	28.00(0.00)	53.42(0.05)	52.57(0.19)	35.00(0.00)	62.33(0.05)	59.44(0.76)	42.02(0.00)
	IMVC/CI(TNNLS'24)	13.56(0.08)	13.31(0.12)	12.32(0.24)	19.18(0.10)	18.36(0.15)	16.58(0.31)	24.46(0.33)	24.14(0.12)	22.23(0.64)
	BWIC/TIMC(TMM'25)	35.69(1.65)	32.37(1.53)	11.59(0.11)	55.81(0.76)	54.61(1.31)	13.79(0.25)	43.06(2.26)	39.21(1.77)	18.24(0.46)
	PBDAL(TMM'25)	49.30(0.84)	47.51(0.97)	47.43(0.69)	45.88(1.61)	43.41(1.68)	42.28(1.96)	52.77(2.35)	51.91(1.64)	51.05(2.32)
	CAL(IJCAI'25)	48.65(2.11)	40.47(1.92)	28.33(2.76)	64.26(0.88)	60.67(0.95)	49.79(1.47)	57.00(2.68)	51.54(1.74)	40.77(3.25)
	ASCR(AAAI'25)	65.67(1.19)	61.60(0.38)	60.90(1.16)	71.73(0.46)	70.74(0.48)	**67.37(0.92)**	71.64(0.94)	67.81(0.86)	66.43(0.72)
	GUITAR(NIPS'26)	46.43(0.87)	45.92(0.80)	45.16(0.20)	42.72(0.69)	41.82(0.71)	40.98(0.27)	51.00(0.86)	50.09(0.94)	49.65(0.72)
	UGMCA(TCE'26)	37.45(1.27)	34.86(1.03)	23.91(0.58)	48.92(1.15)	46.38(0.91)	33.67(0.64)	45.36(1.42)	42.71(1.08)	30.84(0.73)
	OIMC-IAGD(KBS'26)	40.72(2.86)	39.97(0.65)	39.59(0.43)	44.62(1.37)	44.99(0.39)	44.52(0.25)	48.80(1.56)	48.47(0.60)	47.63(0.32)
	Ours	**71.65(0.59)**	**68.39(2.07)**	**62.45(0.43)**	**72.50(0.12)**	**71.52(0.68)**	64.18(0.58)	**74.05(0.25)**	**72.73(0.45)**	**66.84(0.77)**

5.3 THE COMPREHENSIVE STUDY

Visualization: To intuitively evaluate the discriminative ability of the learned representation, we use heatmap and t-SNE to visualize the consensus graphs and spectral embeddings. As shown in Fig. 4, the learned representations exhibit a distinct block diagonal structure on ALOI, BBC4 and compact clusters on COIL, Leaves. Samples belonging to the same cluster are tightly gathered while those from different clusters are well-separated. These results demonstrate that our method effectively enhances intra-cluster compactness and inter-cluster separability across diverse datasets.

Parameters Analysis: We analyze the sensitivity of the proposed method to parameters α, β, and γ on ALOI and Leaves datasets. Here, α controls sparse error regularization, β balances consistency

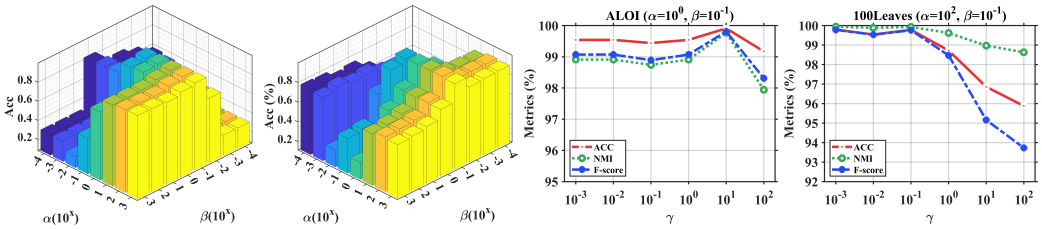

(a) ALOI(γ = 10) (b) Leaves($\gamma = 10^{-3}$) (c) α = 1 and β = 0.1 (d) α = 100 and β = 0.1

Figure 5: The analysis results of the trade-off parameters α, β, and γ on Leaves and ALOI.

between view-specific and consensus graphs, and γ regulates cross-view diversity. As shown in Fig. 5, moderate values of α and β generally yield better performance, as too small values fail to remove noise effectively while overly large values may suppress useful information. Regarding γ, Leaves and ALOI perform best and remain robust over a broad range, indicating stronger redundancy among its views. Overall, the proposed method achieves strong and stable clustering performance across broad parameter ranges, confirming its robustness.

Convergence Analysis: To evaluate convergence, we report the objective value and clustering accuracy (ACC) over iterations on the BBC4 and Caltech101-20 datasets with 30% missing ratio. As shown in Fig. 3, the objective values decrease monotonically and stabilize after about 10 iterations while ACC increases from about 0.6 to nearly 1.0 on BBC4. On Caltech101-20, a similar trend is observed, with the objective converging near zero and ACC reaching about 0.9. The results indicate that the algorithm converges stably and quickly, typically within 15 iterations.

5.4 Ablation Study

To evaluate the contribution of each component in RMTC, we construct three variants: RMTC-E replaces the proposed correlation modeling with a Euclidean-distance-based strategy, RMTC-D removes the tensorial diversity embedding; and RMTC-T removes the tensor regularization term. As reported in Table 3, the performance degradation of RMTC-E demonstrates the advantage of Spearman correlation modeling, while the results of RMTC-D verify that the diversity constraint helps preserve complementary view-specific information. RMTC-T generally suffers the most significant degradation, especially at high missing rates, which demonstrates that tensor regularization is crucial for capturing high-order cross-view correlations and recovering information under severe incompleteness. The complete RMTC achieves the best results under different missing rates, confirming the effectiveness and complementarity of these components.

Table 3: ACC (%) on three benchmark datasets. The best results are shown in **bold**.

	ALOI			Leaves			COIL		
Variant/MR	0.1	0.3	0.5	0.1	0.3	0.5	0.1	0.3	0.5
RMTC-E	93.90	84.03	81.32	91.01	89.53	89.15	85.44	84.80	83.71
RMTC-D	96.44	95.87	94.52	93.23	89.46	84.15	83.86	82.60	81.01
RMTC-T	91.20	86.23	84.37	88.12	87.50	86.94	77.39	69.44	61.32
RMTC	**98.05**	**97.58**	**95.26**	**98.46**	**97.28**	**93.36**	**87.52**	**86.51**	**85.26**

6 Conclusion

This paper proposed RMTC-GL for IMVC. It employs non-parametric Spearman correlation to capture nonlinear sample relationships and a masked graph recovery mechanism to estimate missing correlations while preserving the observed structures. Moreover, tensorial cross-view graph diversity maintains view-specific discriminative information, while multi-tensor enhanced consensus learning jointly exploits cross-view complementarity and high-order consistency to obtain a reliable consensus graph. Extensive experiments on six benchmark datasets demonstrate that RMTC-GL outperforms state-of-the-art methods under different missing rates. The results further confirm its robustness and adaptability to datasets with diverse and complex clustering structures.

AI USE STATEMENT

No generative AI tools are used in any stage of this work, including research design, methodology development, experimental implementation, data analysis, and manuscript preparation. All content is independently produced and reviewed by the authors. We take full responsibility for the final content of this work.

REPRODUCIBILITY STATEMENT

To ensure reproducibility, we will make the source code publicly available upon acceptance of the paper.

REFERENCES

Thibaut Beghin, James S. Cope, Paolo Remagnino, and Sarah Barman. Shape and texture based plant leaf classification. In *Advanced Concepts for Intelligent Vision Systems - 12th International Conference*, volume 6475, pp. 345–353, 2010.

Bing Cai, Gui-Fu Lu, Xiaoxing Guo, and Tong Wu. Tensorized latent representation with automatic dimensionality selection for multi-view clustering. *Pattern Recognition*, 160:111192, 2025.

Jie Chen, Zhu Wang, Hua Mao, and Xi Peng. Low-rank tensor learning for incomplete multiview clustering. *IEEE Transactions on Knowledge and Data Engineering*, 35(11):11556–11569, 2022.

Yawei Chen, Huibing Wang, Jinjia Peng, and Yang Wang. Anchor learning with potential cluster constraints for multi-view clustering. In *Proceedings of the AAAI Conference on Artificial Intelligence*, volume 39, pp. 15939–15947, 2025.

Zhikui Chen, Meng Liu, Yuzhe Li, Hao Zheng, Zhenjiao Liu, Hongwei Zhang, and Liang Zhao. Double-incomplete multi-view clustering with self-induced semantic label diffusion. *Information Sciences*, 753:123626, 2026.

Jie Cui, Yun Fu, Chao Huang, and Jie Wen. Low-rank graph completion-based incomplete multiview clustering. *IEEE Transactions on Neural Networks and Learning Systems*, 35(6):8064–8074, 2024.

Quanxue Gao, Pu Zhang, Wei Xia, Deyan Xie, Xinbo Gao, and Dacheng Tao. Enhanced tensor rpca and its application. *IEEE transactions on pattern analysis and machine intelligence*, 43(6): 2133–2140, 2020.

JM Geusebroek, GJ Burghouts, and AWM Smeulders. The amsterdam library of object images. *International Journal of Computer Vision*, 61(1):103–112, 2005.

Derek Greene and Padraig Cunningham. Practical solutions to the problem of diagonal dominance in kernel document clustering. In *Proceedings of International Conference on Machine Learning*, volume 148, pp. 377–384, 2006.

Z Gu, Z Zhong, X Zhang, and B Li. Constant degree matrix-driven incomplete multi-view clustering via connectivity-structure and embedding tensor learning. In *Proceedings of International Conference on Learning Representations*, 2026.

Wei Guo, Hangjun Che, Man Fai Leung, Long Jin, and Shiping Wen. Robust mixed-order graph learning for incomplete multi-view clustering. *Information Fusion*, 115(000), 2025.

XiaoXing Guo and Gui-Fu Lu. Tensor-based global block-diagonal structure radiation for incomplete multiview clustering. *Expert Systems with Applications*, 255:124788, 2024.

Shizhe Hu, Jiahao Fan, Guoliang Zou, and Yangdong Ye. Multi-aspect self-guided deep information bottleneck for multi-modal clustering. In *Proceedings of the AAAI Conference on Artificial Intelligence*, volume 39, pp. 17314–17322, 2025a.

Shizhe Hu, Binyan Tian, Weibo Liu, and Yangdong Ye. Self-supervised trusted contrastive multi-view clustering with uncertainty refined. In *Proceedings of the AAAI Conference on Artificial Intelligence*, volume 39, pp. 17305–17313, 2025b.

Enze Ji, Xuan Chen, Zhikui Chen, and Chuan Xiao. Incomplete multi-view clustering via imbalanced anchor-aligned graph learning. *Pattern Recognition*, pp. 114290, 2026a.

Enze Ji, Zhikui Chen, Anni Chen, and Huicen Guo. Decomposed tensorized graph learning with representation-induced view recovery for federated incomplete multi-view clustering. *Neurocomputing*, 701:134605, 2026b.

Enze Ji, Meng Liu, Yuzhe Li, and Zhikui Chen. Content-style disentanglement guided representation learning for deep incomplete multi-view clustering. In *Proceedings of the Thirty-Fifth International Joint Conference on Artificial Intelligence*, pp. 4394–4402, 2026c.

Xiaosha Li, Qianqian Sun, Zhaoliang Ren, and Yiming Sun. Dynamic incomplete multi-view imputing and clustering. In *Proceedings of the 30th ACM International Conference on Multimedia*, pp. 3412–3420, 2022a.

Xingfeng Li, Yuangang Pan, Yuan Sun, Quansen Sun, Yinghui Sun, Ivor W Tsang, and Zhenwen Ren. Incomplete multi-view clustering with paired and balanced dynamic anchor learning. *IEEE Transactions on Multimedia*, 27:1486–1497, 2025.

Zhenglai Li, Chang Tang, Xiao Zheng, Xinwang Liu, Wei Zhang, and En Zhu. High-order correlation preserved incomplete multi-view subspace clustering. *IEEE Transactions on Image Processing*, 31:2067–2080, 2022b.

Cheng Liu, Rui Li, Si Wu, Hangjun Che, Dazhi Jiang, Zhiwen Yu, and Hau-San Wong. Self-guided partial graph propagation for incomplete multiview clustering. *IEEE Transactions on Neural Networks and Learning Systems*, 35(8):10803–10816, 2023.

Cheng Liu, Rui Li, Hangjun Che, Man-Fai Leung, Si Wu, Zhiwen Yu, and Hau-San Wong. Latent structure-aware view recovery for incomplete multi-view clustering. *IEEE Transactions on Knowledge and Data Engineering*, 36(12):8655–8669, 2024.

Jiyuan Liu, Xinwang Liu, Yi Zhang, Pei Zhang, Wenxuan Tu, Siwei Wang, Sihang Zhou, Weixuan Liang, Siqi Wang, and Yuexiang Yang. Self-representation subspace clustering for incomplete multi-view data. In *Proceedings of the ACM International Conference on Multimedia*, pp. 2726–2734, 2021.

Qian Liu, Huibing Wang, Jinjia Peng, Yawei Chen, Mingze Yao, Xianping Fu, and Yang Wang. Consensus-guided incomplete multi-view clustering via cross-view affinities learning. In *Proceedings of the International Joint Conference on Artificial Intelligence*, pp. 5761 –5769, 2025.

Tingjin Luo, Yueying Liu, Xinyue Zhang, and Chenping Hou. Non-convex transfer subspace learning via embedded distribution alignment. *IEEE Transactions on Image Processing*, 2026.

Wei Lv, Chao Zhang, Huaxiong Li, Xiuyi Jia, and Chunlin Chen. Joint projection learning and tensor decomposition-based incomplete multiview clustering. *IEEE Transactions on Neural Networks and Learning Systems*, 2023.

Xuanlong Ma, Yanhong She, Shixun Lin, Fenfang Xie, Xuhang Chen, Ting Shu, and Guo Zhong. Unified grassmann manifold-based completion and alignment for incomplete multi-view clustering. *IEEE Transactions on Consumer Electronics*, 2026.

Sameer A Nene, Shree K Nayar, Hiroshi Murase, et al. Columbia object image library (coil-20). Technical report, Technical report CUCS-005-96, 1996.

Qingyang Shu, Mingchang Cheng, Jianmei Ren, Tiefeng Ma, and Aihua Han. Step-wise incomplete multi-view clustering through joint utilization of structure and completion graphs. *Information Fusion*, pp. 104268, 2026.

Jiayi Tang, Long Zhao, and Xinwang Liu. Incomplete multiview clustering based on consensus information. *IEEE Transactions on Neural Networks and Learning Systems*, 36(5):8317–8330, 2024.

Bocheng Wang, Chusheng Zeng, Mulin Chen, and Xuelong Li. Towards learnable anchor for deep multi-view clustering. In *Proceedings of the AAAI Conference on Artificial Intelligence*, volume 39, pp. 21044–21052, 2025.

Jie Wen, Zheng Zhang, Zhao Zhang, Lei Zhu, Lunke Fei, Bob Zhang, and Yong Xu. Unified tensor framework for incomplete multi-view clustering and missing-view inferring. In *Proceedings of the AAAI conference on artificial intelligence*, volume 35, pp. 10273–10281, 2021.

Jinghan Wu, Rankun Chen, Haoran Wang, Xuetao Zhang, Ben Yang, and Badong Chen. One-step incomplete multi-view clustering via imputed anchor graph discretization. *Knowledge-Based Systems*, pp. 114935, 2026.

Tingting Wu, Zhendong Li, Zhibin Gu, Jiazheng Yuan, and Songhe Feng. Koala: Kernel coupling and element imputation induced multi-view clustering. In *Proceedings of the AAAI Conference on Artificial Intelligence*, pp. 21581–21589, 2025.

Deng Xu, Chao Zhang, Cong Guo, Chunlin Chen, and Huaxiong Li. Fast incomplete multi-view clustering with adaptive similarity completion and reconstruction. In *Proceedings of the AAAI Conference on Artificial Intelligence*, pp. 21734–21742, 2025.

Mingze Yao, Huibing Wang, Yawei Chen, and Xianping Fu. Between/within view information completing for tensorial incomplete multi-view clustering. *IEEE transactions on multimedia*, 27: 1538–1550, 2025.

Yu Yun, Jing Li, Quanxue Gao, Ming Yang, and Xinbo Gao. Low-rank discrete multi-view spectral clustering. *Neural Networks*, 166:137–147, 2023.

Chao Zhang, Jingwen Wei, Bo Wang, Zechao Li, Chunlin Chen, and Huaxiong Li. Robust spectral embedding completion based incomplete multi-view clustering. In *Proceedings of the ACM international conference on multimedia*, pp. 300–308, 2023.

Zhenhao Zhong, Zhibin Gu, Pengpeng Yang, Ruiqiang Guo, et al. Gaussian regression-driven tensorized incomplete multi-view clustering with dual manifold regularization. *Advances in Neural Information Processing Systems*, 38:72102–72131, 2026.

Baishun Zhou, Jintian Ji, Zhibin Gu, Zihao Zhou, Gangyi Ding, and Songhe Feng. One-step graph-based incomplete multi-view clustering. *MULTIMEDIA SYSTEMS*, 30(1), 2024.